THE ASTROPHYSICAL JOURNAL, 416:51–61, 1993 October 10

3C 317: AN AMORPHOUS RADIO SOURCE IN THE COOLING FLOW CLUSTER ABELL 2052

JUN-HUI ZHAO,[1] DEAN M. SUMI,[2] J. O. BURNS,[3] AND NEBOJSA DURIC[4]
Received 1993 February 25; accepted 1993 April 21

ABSTRACT

We have observed the radio source 3C 317 in the X-ray cooling flow cluster A2052 using the VLA at wavelengths 90, 20, 6, and 3.6 cm. Unlike most moderate-power extragalactic radio sources, 3C 317 is characterized by a compact core and an amorphous halo with an angular size of 75″ × 45″. The spectrum of the halo emission is unusually steep ($\alpha_{20/90\,\mathrm{cm}} \sim -1.5$ and $\alpha_{6/20\,\mathrm{cm}} \sim -1.9$). Surrounding the compact radio core at the center of the galaxy, a bipolar structure has been observed indicating that an outflow may have been initially collimated to some degree. However, no well-collimated jets have been detected with a resolution of 0″.3. The lack of strong collimation could be due to jet disruption in the cooling flow on scales unresolved by the VLA observations. An observed gradient of spectral index from flat ($\alpha \sim -0.05$) at the nucleus to steep in the halo ($\alpha \sim -1.9$) also favors the hypothesis that relativistic electrons originated within the active nucleus and "aged" as they move outward. The radio morphology, the curved spectrum of the integrated flux density, and the gradient within the spectral index distribution suggest that diffusion, synchrotron losses and electron reacceleration likely play important roles in the transport of the relativistic electrons from the nucleus to the radio halo. In addition, our new observations reveal that the halo was a wealth of substructures: a loop (25 kpc × 1.5 kpc) and large-scale filaments which connect to the bipolar structure. Linear analysis suggests that these filamentary structures could form by either magnetic field reconnection or Rayleigh-Taylor instabilities. The details of this peculiar radio source provide evidence that radio plasma interacts with X-ray cooling flows in the centers of clusters.

Subject headings: cooling flows — galaxies: clusters: individual (Abell 2052) — galaxies: jets — galaxies: structure — radio continuum: galaxies

1. INTRODUCTION

Distributions of X-ray surface brightness in some clusters of galaxies obtained from the *Einstein* X-ray observatory are strongly peaked in the cluster cores, suggesting the presence of cooling flows (Jones & Forman 1984; Stewart et al. 1984). The global properties of these cooling flow clusters have been discussed in recent reviews (Fabian, Nulsen, & Canizares 1991; Sarazin 1986). The radiative cooling time of the central gas is 10^9 yr, substantially shorter than the Hubble time. Cooling flows in clusters may be quite common, occurring in 70%–90% of rich clusters (Edge, Stewart, & Fabian 1992). The estimated rates of mass accretion in the cooling core (radius ~50–300 kpc) are typically 100 $M_\odot$ yr^{-1}. In addition, high angular resolution X-ray images of the cluster A2029 observed with the *ROSAT* HRI suggest that the cooling flow is likely aspherical (Sarazin et al. 1992).

Many of these cooling flow clusters have a central dominant galaxy which is associated with a radio source (Burns 1990). The radio morphologies and linear sizes of the dominant radio galaxies in cooling flows, such as 3C 84 (Burns et al. 1992), significantly differ from the wide-angle tailed and narrow-angle tailed radio sources which are common in clusters of galaxies (Burns 1990; Zhao, Burns, & Owen 1989). The X-ray cooling inflows may be dynamically important in distorting radio outflows ejected from nuclei and confining the radio plasma into a small volume.

The radio source 3C 317 is associated with the dominant galaxy UGC 9799 in the Abell cluster 2052. *Einstein* X-ray images show that there is a significant central X-ray excess in A2052 (e.g., Burns 1990), which indicates an X-ray cooling inflow with a mass accretion rate of approximately 130 $M_\odot$ yr^{-1} in the central region (Arnaud 1990). 3C 317 has an intermediate radio power of 10^{25} W Hz^{-1} at 20 cm which marks the transition between the structural classes of radio galaxies FR I and FR II (Faranoff & Riley 1974; Bridle & Perley 1984). Unlike most moderate power extragalactic sources, 3C 317 is not characterized by jets or lobes, suggesting a well-collimated outflow. Instead, earlier VLA observations (Roland et al. 1985; Baum et al. 1988; Zhao et al. 1989; Burns 1990) have shown a fundamentally different morphology consisting of an amorphous halo surrounding a bright core that is coincident with the optical center of the galaxy. In addition, Baum et al. (1988) found several optical extended emission-line filaments that are cospatial with the radio emission. This may suggest a possible connection between the radio plasma and the optical filaments. The phenomena found in 3C 317 provide substantial evidence for the interaction between the different components of gas at the cluster center.

3C 317 is one of the best candidates for a detailed study of these amorphous sources because of its closeness ($z = 0.0345$) and relatively low dynamic range requirements. In § 2, we briefly discussed our new VLA observations and data reductions for 3C 317. In § 3, we present the results obtained from the images at 90, 20, 6, and 3.6 cm. We discuss plausible explanations for the radio halo and the substructure within

[1] National Radio Astronomy Observatory, P.O. Box O, Socorro, NM 87801. The National Radio Astronomy Observatory is operated by Associated Universities, Inc., under cooperative agreement with the National Science Foundation. Also Institute for Astrophysics, Department of Physics and Astronomy, University of New Mexico.

[2] National Center for Supercomputing Applications, University of Illinois, Urbana-Champaign, Urbana, IL 61801.

[3] Department of Astronomy, New Mexico State University, Box 30001/Dept. 4500, Las Cruces, NM 88003.

[4] Institute for Astrophysics, Department of Physics and Astronomy, University of New Mexico, Albuquerque, NM 87131.

this amorphous radio source (§ 4). In this paper, we assume $H_0 = 50$ km s^{-1} Mpc^{-1}, so the scale is ≈ 1 kpc per arcsec.

2. OBSERVATIONS AND DATA REDUCTIONS

A summary of the VLA observational parameters is given in Table 1. The date of the observations is given in column (1). The VLA configuration is given in column (2). The observing frequencies and bandwidths are given in columns (3) and (4), respectively. The primary calibrator used to determine the flux density scale and the calibrator's flux density at each frequency are presented in columns (5) and (6), respectively. The field center for all the observations of 3C 317 was R.A. = $15^h14^m17^s.00$, decl. = 07°12′18″.0 (epoch 1950). The absolute flux density for 3C 317 was calibrated by observing 3C 286, for 5 minutes at the beginning and the end of the observing runs. The flux density of 3C 286 is on the Baars et al. (1977) scale. At 20, 6, and 3.6 cm, the secondary calibrator 1502+106 was observed for 1.5 minutes every 20 minutes to track the phase errors caused by changing atmospheric and system conditions over the configuration. At 90 cm, a VLA continuum mode was used for the observations. The phase and amplitude were calibrated using the compact source 1416+067.

At each frequency, the A configuration data base was initially deconvolved using the CLEAN algorithm (Clark 1980), and self-calibration techniques were applied in order to correct for antenna-based phase and amplitude errors (Cornwell 1986). The model of 3C 317 generated from the clean components of the final A configuration image was used to correct the B and C configuration data bases. The final images at 3.6, 6, 20, and 90 cm were deconvolved using the maximum entropy algorithm, VTESS (Cornwell 1986). In order to see the extended structures with different resolution, we tapered some of the image visibilities to produce low resolution images. The final rms noise for each image is within a factor of 2 of the theoretical thermal noise level. The parameters of the final maps are given in Table 2.

3. RESULTS

3.1. *Continuum Brightness Distribution*

Figure 1 shows the largest scales of structure in 3C 317 from 90 cm observations using the VLA in the A configuration with a resolution of 5″. The source is well represented by a core-halo emission elongated in the south-north direction with an angular size of 75″ × 45″.

Figure 2 (Plate 1) shows an image at 20 cm made by combining the visibility data from the A, B, and C configurations with a resolution of 1″.4. At this resolution, these new observations show several interesting features in this amorphous halo. In general, 3C 317 is characterized by a compact core, a bipolar emission structure oriented in the north-south direction, and an amorphous halo, in agreement with previous results (Baum et al. 1989; Burns 1990). However, a number of filaments 20″ north of the nucleus and a loop 15″ northeast of the nucleus have been revealed in this new image for the first time (see Fig. 2).

These features are also observed at 6 cm with a similar resolution. Figure 3 shows a comparison between the radio images at 5 GHz (Fig. 3*a*) and 1.5 GHz (Fig. 3*b*).

Finally, in order to better resolve the substructures, we have made a map with the combined A, B, and C configuration observations at 6 cm with a resolution 0″.4 (Fig. 4). Most of the halo is resolved at this resolution. The substructures in the radio halo are labeled in Figure 4.

TABLE 1

OBSERVATION LOG

Date (1)	Array (2)	Frequency (GHz) (3)	Bandwidth (MHz) (4)	Calibrator (5)	S[a] (Jy) (6)
1988 Nov 30	A	0.33	3.125	3C 286	26.77
1988 Dec 1	A	1.5	50	3C 286	14.51
1989 Mar 30	B	1.5	50	3C 286	14.51
1989 Jun 26	C	1.5	50	3C 286	14.51
1988 Dec 1	A	4.9	50	3C 286	7.31
1989 Mar 30	B	4.9	50	3C 286	7.31
1989 Jun 26	C	4.9	50	3C 286	7.31
1988 Nov 30	A	8.4	50	3C 286	5.18

[a] Total flux density of 3C 286 based on the Baars et al. 1977 scale.

TABLE 2

PARAMETERS OF THE IMAGES[a]

λ (cm)	Arrays	rms (mJy beam^{-1})	Beam Size (FWHM)	Figures
90	A	2.5	5″.0 × 5″.0	1
20	A + B + C	0.040	1.48 × 1.36	2, 3*b*
6	B + C	0.015	1.48 × 1.36	3*a*
6	A + B + C	0.015	0.42 × 0.41	4*a*, 4*b*

[a] The final images are made using the maximum entropy method (MEM) (see Cornwell 1986).

3.2. *Notes on Individual Components*

3.2.1. *The Compact Core*

At the center of the radio source, there is a strong compact component ($\sim$0.3 Jy at $\lambda \leq 20$ cm), coincident with the optical nucleus of this galaxy. This compact source marks the active nucleus of this galaxy and possibly the center of the cluster A2052. At 20 cm and shorter wavelengths, the VLA observations are able to separate the compact source from the extended halo emission. At 90 cm, we are not able to isolate the compact nuclear source from the confusion of extended emission. We determined the flux densities of the point source at 20, 6, and 3.6 cm (see Table 3). Over the observation period of a half-year, we have found no significant variations of the core flux density at 6 and 20 cm. In addition, a 3.6 cm image of 3C 317, which is not shown in this paper, was made using the A-configuration observations with a resolution of $\sim$0″.3. The compact nuclear source is not resolved and is fitted well with a point source model, while all the surroundings of the core are well resolved at this resolution. No evidence for collimated jets directed from the compact core has been found. The flux densities and the limits on the angular size are given in Table 3.

3.2.2. *The Bipolar Structure*

Instead of collimated jets, there is a bipolar structure surrounding the nucleus that is oriented in the north-south direction. This can be best seen in the high-resolution map in Figure 4. The bipolar structure has a largest angular size of approximately 30″. The northern part of the bipolar structure consists of a lobe with a peak in the surface brightness approximately 5″ north of the nucleus. This peak is connected to the nucleus by a ridge on the eastern side of the lobe. The overall structure of the lobe suggests a bubble seen in projection. The southern part of the bipolar structure consists of a curved plume. This is

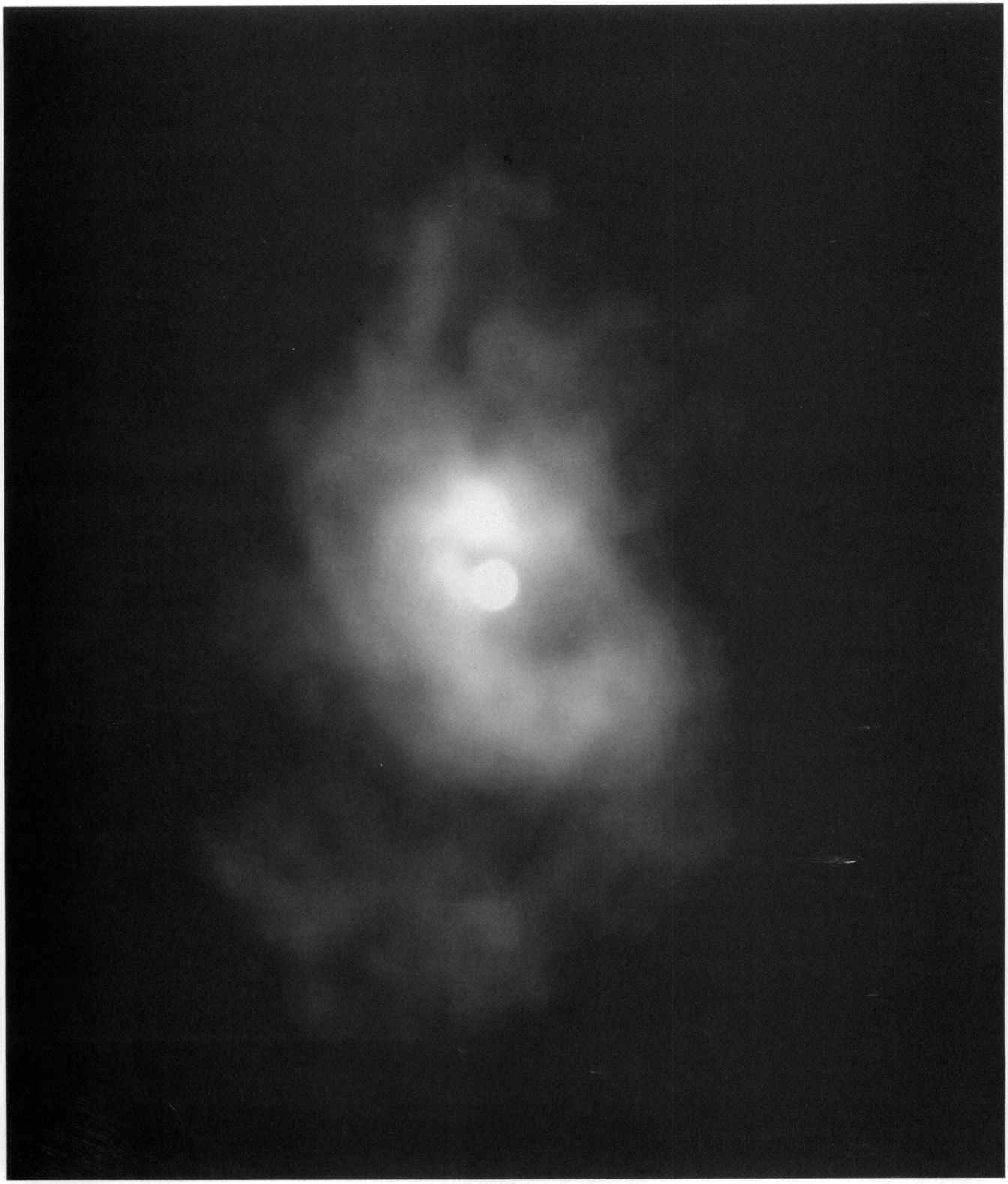

FIG. 2.—Gray-scale image of 3C 317 at 20 cm, showing a compact source at the center and the curved bipolar component surrounded by a diffuse halo. The filaments and loop seen in this image are also shown in 6 cm image (see Fig. 4). The image were convolved to 1″.4. A contour map of this image is shown in Fig. 3*b*.

ZHAO et al. (see 416, 52)

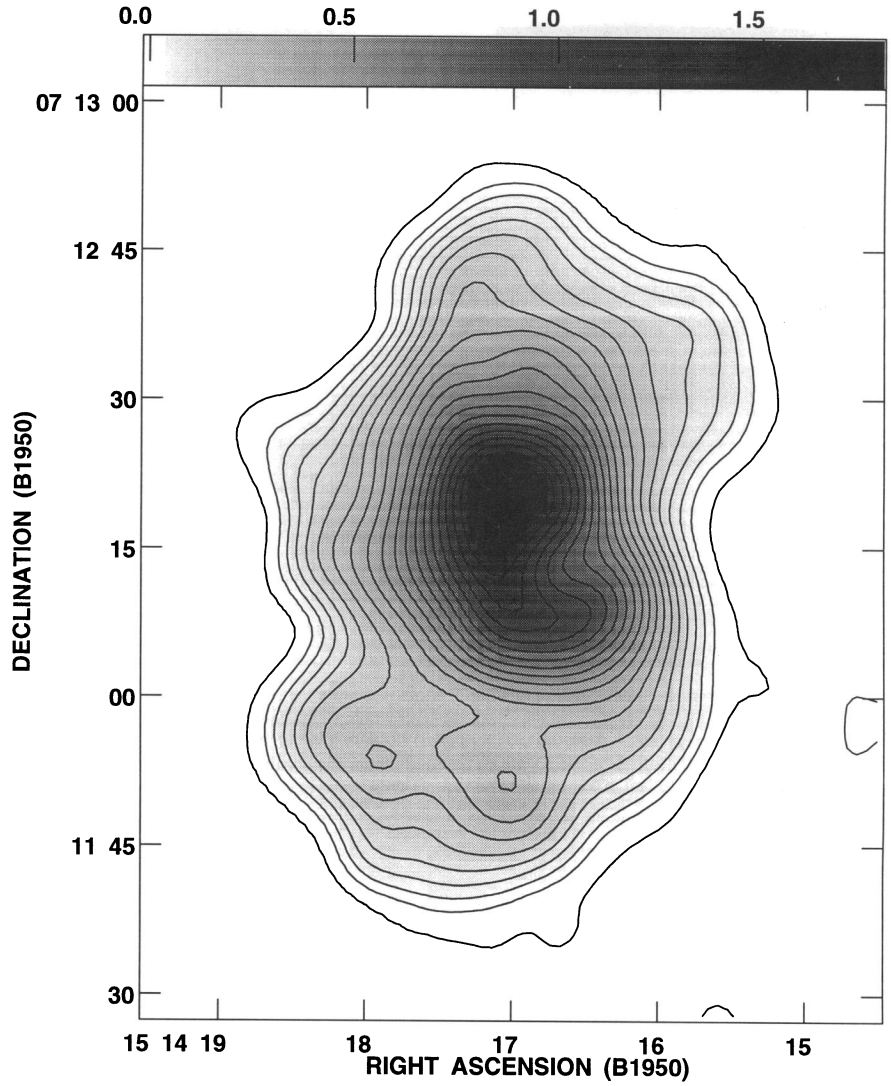

FIG. 1.—Gray-scale representation of a 90 cm image made from VLA observations in the A configuration. The gray-scale range of the flux density is 0 ~ 1.8 Jy beam^{-1}. The contours are −14, 14, 35, 56, 84, 119, 161, 210, 266, 329, 399, 476, 560, 651, 749, 854, 966, 1085, 1211, 1344, and 1484 mJy beam^{-1}. The FWHM size of beam is 5″ × 5″. The typical rms noise is about 2.5 mJy beam^{-1}.

the closest feature in 3C 317 to a jet structure. This feature does not appear to be directly connected with the nucleus, however. The flux densities of the bipolar component, given in Table 3, were determined by integrating the emission from the region defined roughly by contour levels of 0.6 and 5 mJy beam^{-1} in the 6 and 20 cm images (or Figs. 3*a* and 3*b*), respectively, excluding the contributions from the compact nuclear core, the halo, and the major filaments (the loop and northern filament).

3.2.3. *Loop and Filaments*

The bipolar structure is surrounded by a more or less amorphous halo. High-resolution observations (see Fig. 4) show that the halo consists of considerable amounts of substructure. To the east, there is loop structure that is connected with the northern lobe and the southern plume. This loop is approximately 25″ in length. The loop is slightly resolved

TABLE 3

RADIO COMPONENTS OF 3C 317

COMPONENT	S (Jy) 20 cm	6 cm	3.6 cm	$\alpha_{6/20\,cm}$	ANGULAR SIZE
Core	0.33±0.01	0.31±0.01	0.27±0.01	−0.05±0.03	<0″.3
Bipolar	2.2±0.1	0.31±0.02	...	−1.64±0.1	30″ × 15″
Halo	2.8±0.2	0.30±0.02	...	−1.9±0.1	75 × 45
Loop	0.11±0.01	0.017±0.003	...	−1.6±0.1	25 × 1.5
Filament	0.081±0.007	0.013±0.002	...	−1.5±0.1	20 × 2

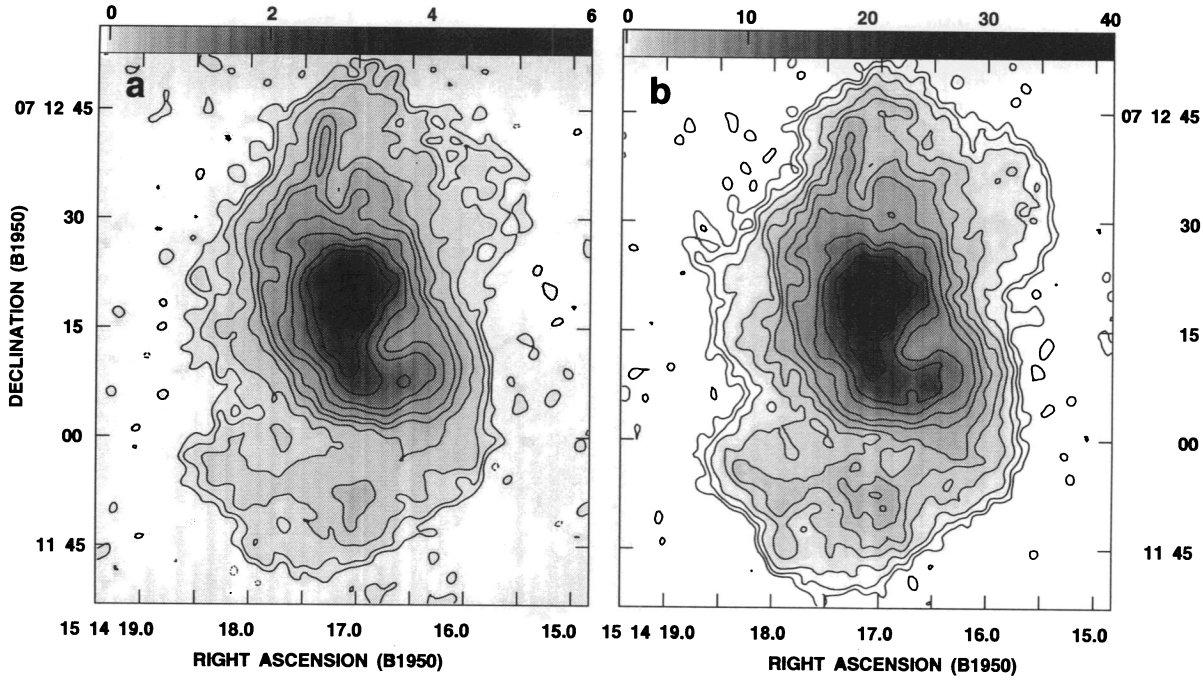

FIG. 3.—Comparison of the radio halo between 6 and 20 cm. (*a*) The left-hand panel is a gray-scale representation of the 6 cm image made from the combined visibility data of the B and C configurations using the VLA. The typical rms noise is 15 μJy beam^{-1}. The beam size (FWHM) is 1″.48 × 1″.36. The gray-scale range of the flux density is −0.1 to 6 mJy beam^{-1}. The contours are −0.04, 0.04, 0.08, 0.16, 0.32, 0.48, 0.64, 0.96, 1.28, 1.92, 2.56, 3.84, 5.12, 6.40, 7.68, 10.3, and 20.5 mJy beam^{-1}. (*b*) The right-hand panel is a gray-scale representation of the 20 cm image made from the combined visibility data of the A and B configurations using the VLA with the same beam size as in the 6 cm image in the left-hand panel. The typical rms noise in this image is 40 μJy beam^{-1}. The gray-scale range of the flux density is −0.1 to 40 mJy beam^{-1}. The contours are 0.2, 0.4, 0.8, 1.6, 2.6, 3.2, 4.8, 6.4, 9.6, 12.8, 25.6, 32, 38.4, 51.4, and 102.8 mJy beam^{-1}.

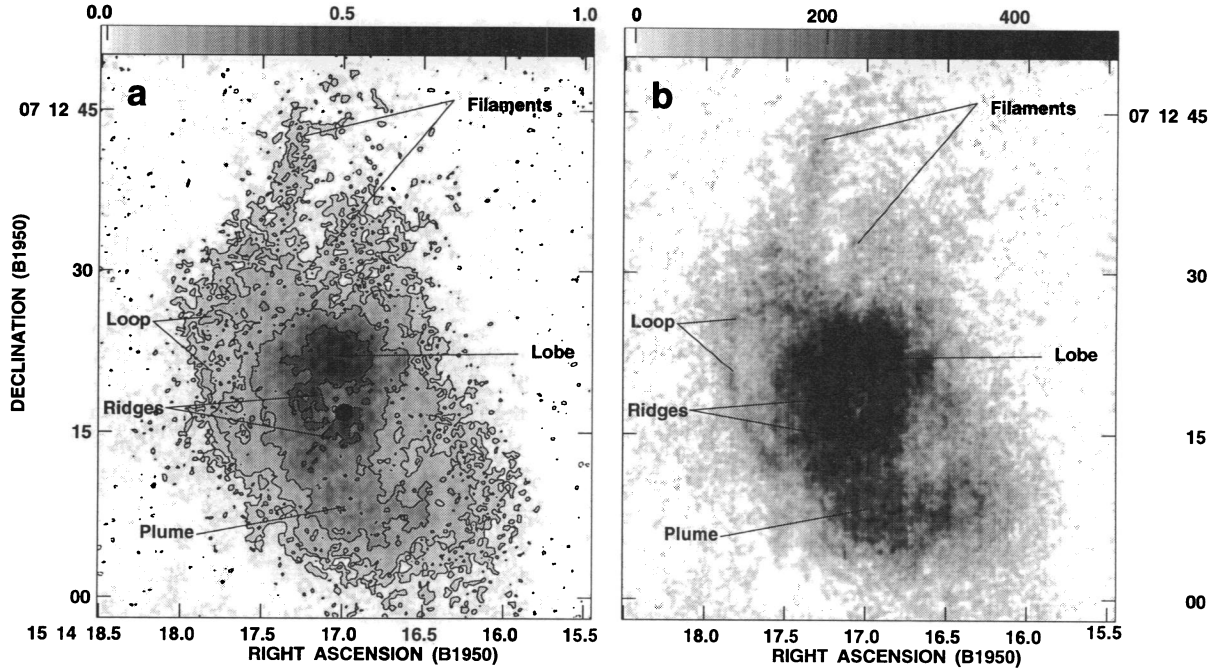

FIG. 4.—Two different gray-scale representations of the 6 cm image made from the combined visibility data of the A, B, and C configurations with a resolution of 0″.4. At this resolution, the halo is well resolved. The bipolar structure, filaments, and loop are shown in two different gray scales. (*a*) The left-hand panel shows the immediate surroundings of the nucleus. The gray-scale range of the flux density is −0.01 to 1 mJy beam^{-1}. The contours are −0.06, 0.06, 0.12, 0.24, 0.48, 0.96, and 1.92 mJy beam^{-1}. (*b*) The right-hand panel is the same image using a gray scale such that the filaments and the loop are shown better. The gray-scale range of the flux density is −0.01 to 0.5 mJy beam^{-1}. The gray-scale representation for the bipolar structure is partially saturated.

(width [FWHM] ~ 1″.5) and has a relative contrast to the surrounding halo emission of approximately 3:1 (at 6 cm).

To the north, there are several filamentary structures. The most prominent filament extends radially outward approximately 15″ before bending toward the west. To the south, there are several substructures in the halo. In contrast to the filamentary structures in the northern part of the halo, these substructures are more clumpy in appearance.

Table 3 gives the flux densities of the components after correcting for the diffuse emission from the halo. The uncertainties of the flux densities are large because the filamentary emission is confused by the diffuse emission from the halo.

3.3. *Distribution of Spectral Index*

In Figure 5, the integrated spectrum of the source is presented using a combination of previous single-dish and interferometer data, and our new VLA measurements (Table 4). A good fit to the spectrum is obtained using two power-law spectra. We find a break frequency around 0.5 GHz; $\alpha \simeq -1.4$ for $\nu > 0.5$ GHz and $\alpha \sim -0.8$ for $\nu < 0.5$ GHz, where $S_\nu \propto \nu^\alpha$.

We show spectral index maps between 6 and 20 cm in Figure 6*a* and between 20 and 90 cm in Figure 6*b* with a resolution of 1″.4 and 5″, respectively. In addition, Figures 7*a* and 7*c* show distributions of the annulus-averaged surface brightness, which were made with annular widths of 1″ in Figure 7*a* and of 2″ in Figure 7*c*, respectively, centered at the core (R.A. = $15^h14^m16^s.99$ and decl. = 7°12′16″.8, epoch 1950). The spectral index profiles in Figures 7*b* and 7*c* were obtained by calculating the spectral index at each annular bin from the annulus-averaged intensities between 6 and 20 cm in Figure 7*a* and between 20 and 90 cm in Figure 7*c*, respectively.

A gradient in spectral index is seen in both 6/20 cm and 20/90 cm spectral index images. At the nucleus, the spectral index is about −0.05. The bipolar structure and the halo are considerably steeper, ranging from −1.6 to −1.7 and from −1.7 to −2.5, respectively. One interesting deviation from this trend is the loop and northern filament. These enhanced emission features have a spectral index of −1.5 (see Table 3). The spectral indices of the loop and filament are based on the images in Figure 3 after corrections for the confusion emission from the halo.

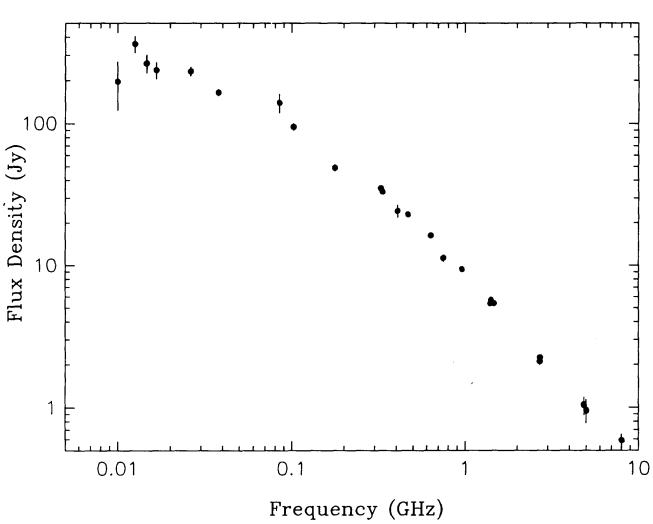

FIG. 5.—The total flux density spectrum in a frequency range between 0.01 and 8 GHz. There appears to be a break around 0.5 GHz. A good fit is obtained using two power laws with $\alpha = -1.4$ for $\nu > 0.5$ and $\alpha = -1.4$ for $\nu < 0.5$.

TABLE 4

TOTAL FLUX DENSITIES OF 3C 317

Frequency (MHz)	S_ν (Jy)	References
10.0	197±73	1
12.6	359±47	1
14.7	263±37	1
16.7	236±31	1
26.3	232±16	2
38	165±8	3, 4
85	140±15	5
103	95±5	6
178	49±2	3, 4
327	35.2±1	7
333	33.3±1	7
408	24.3±2	3
468	23.0±0.5	8
635	16.3±0.3	8
750	11.3±0.6	4
960	9.41±0.2	8
1410	5.70±0.1	8
1469	5.40±0.05	7
2695	2.11±0.10	4
2700	2.25±0.02	8
4835	1.05±0.01	7
5000	0.96±0.18	8
5009	0.95±0.03	8
8000	0.59±0.10	9

REFERENCES.—(1) Braude et al. 1979; (2) Viner and Erickson 1975; (3) Williams et al. 1968; (4) Kellermann et al. 1969; (5) Mills et al. 1958; (6) Gubanov 1985; (7) The VLA measurements from this paper; (8) Wills 1975; (9) Stull 1971.

At 20 and 90 cm, in general, the spectral indices of these components are relatively flat in comparison with those at high frequencies. The bipolar structure ranges from −0.8 to −1.2. The average spectral index in the halo is about −1.5.

3.4. *Comparison of the Radio Emission Distribution with Optical Emission-Line Gas*

Optical emission-line gas has been detected by Baum et al. (1989) demonstrating that this gas ($T_e \sim 10^4$ K) cospatially exists with the radio continuum emission in the central region of the dominant galaxy. Figure 8 shows a detailed comparison of the radio emission (gray-scale) with the optical narrow-band image of Hα + [Ne II] (the contours). The two images are aligned assuming that both optical and radio compact sources correspond to the common nucleus of the galaxy. We find that the extended optical emission-line filaments coincide with relatively weak regions of the radio continuum emission.

3.5. *The Physical Conditions in The Radio Substructures*

Assuming energy equipartition, we estimate minimum *B*-fields and minimum pressures (e.g., Burns, Owen, & Rudnick 1979) in the components listed in Table 3. The calculations are based on the assumptions that (1) the ratio of proton to electron energies is $k \approx 1$; (2) the volume-filling factor is $\Phi = 1$; (3) the lower and higher frequency cutoffs are $\nu_1 = 10^7$ Hz and $\nu_1 = 10^{11}$ Hz, respectively; and (4) cylindrical geometry for all the components is used except for the core for which the spherical geometry is assumed. The calculated equipartition results are given in Table 5.

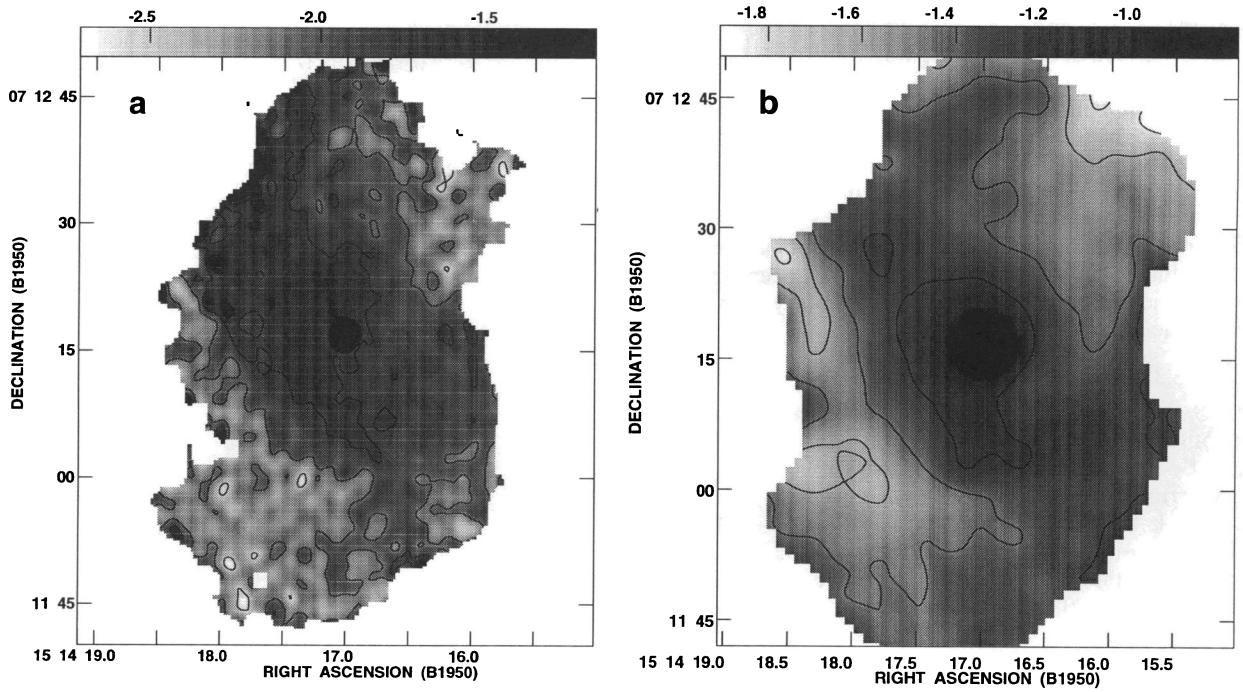

FIG. 6.—(*a*) A gray-scale representation of a spectral index distribution between 20 and 6 cm, made from the images shown in Fig. 3. The gray-scale range of the spectral index is -2.7 to -1.2. (*b*) A gray-scale representation of a spectral index distribution between 90 and 20 cm with a resolution of 5″. The gray-scale range of the spectral index is -1.9 to -0.8.

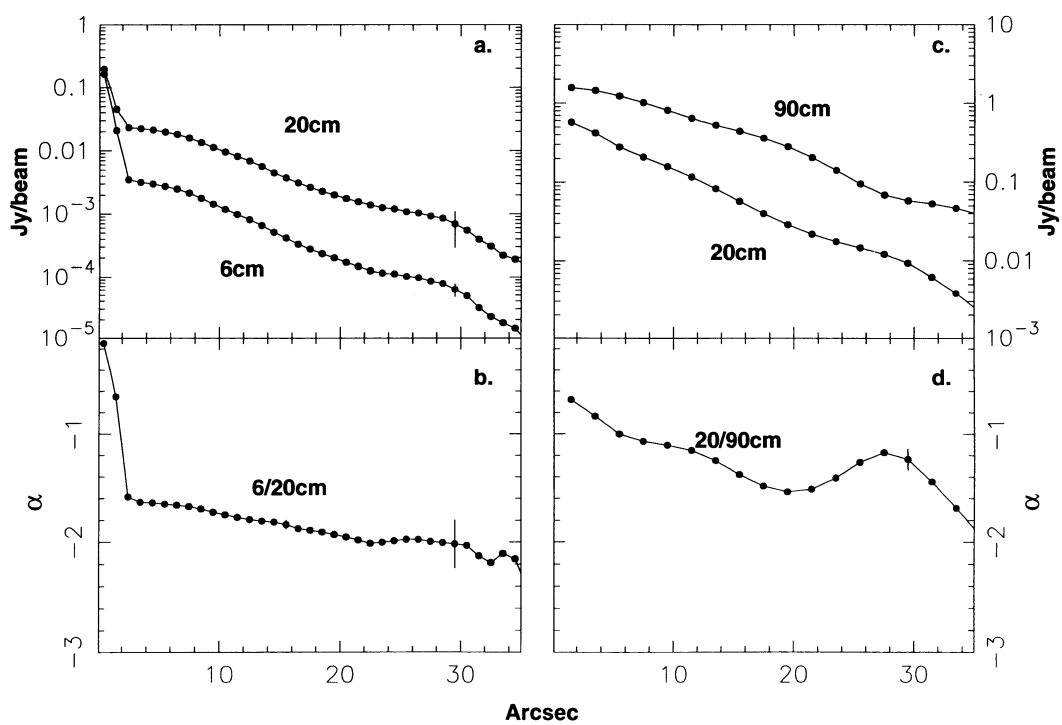

FIG. 7.—(*a*) Profiles of the surface brightness distribution along the radius made from the annulus-average of the images at 6 and 20 cm with a resolution of 1″.4. (*b*) The relevant spectral index profile between the two wavelengths. (*c*) Profiles of surface brightness distribution along the radius made from the annulus-average of the images at 20 and 90 cm with a resolution of 5″. (*d*) The relevant spectral index profile between the two wavelengths. The errors of most data points in above plots are less than the size of the symbols. The typical errors at both radii 15″ and 30″ are indicated.

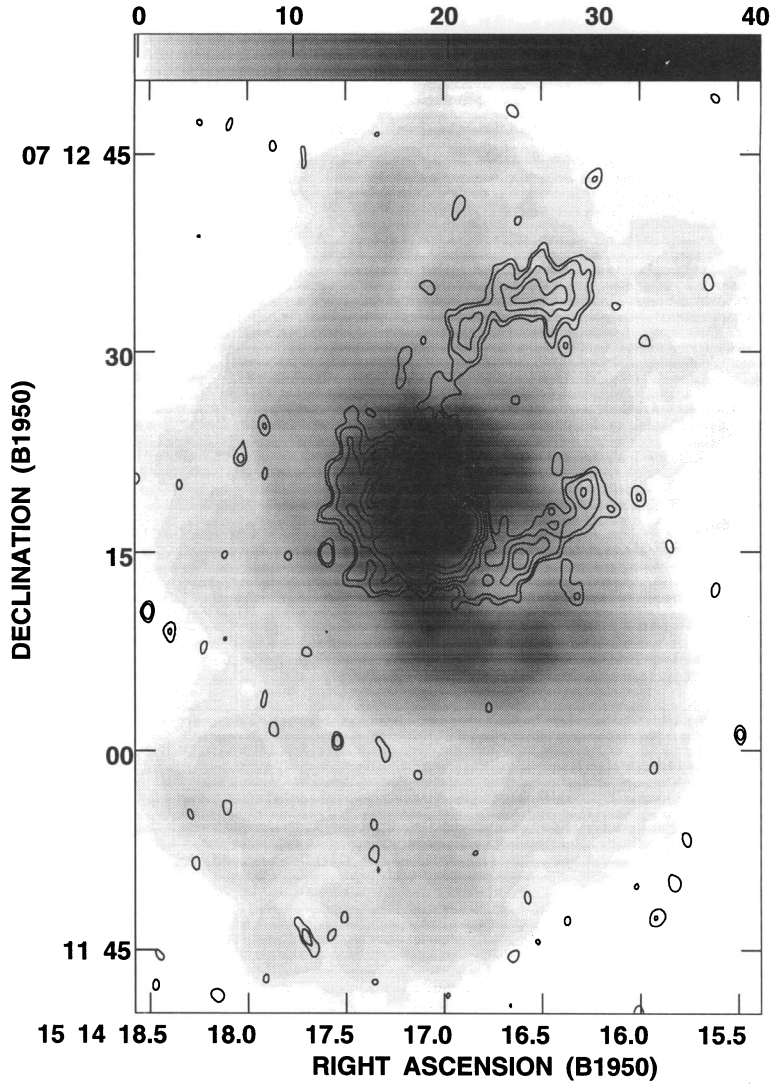

FIG. 8.—Optical emission line Hα + [N II] (contour) (Baum et al. 1989) is superposed on a 20 cm image of 3C 317. The gray-scale representation indicates the radio emission intensity. The gray-scale range of the flux density is −0.1 to 40 mJy beam^{-1}.

It is interesting to compare the minimum total pressure derived from the radio data with the thermal pressure inferred from the deprojections of the X-ray data. The physical conditions of the ambient X-ray gas in the cooling core of Abell 2052 were calculated by Arnaud (1990) from an *Einstein* X-ray image. The central pressure, $p \approx n_e k T_e$, can be determined from the deconvolved density ($n_e \sim 0.01$ cm^{-3}) and temperature ($T_e \sim 1 \times 10^7$ K) within a cooling core of ~100 kpc derived from the HRI X-ray image (Arnaud 1990). The resulting thermal pressure of 2×10^{-11} dyn cm^{-2} is compatible with the minimum pressure determined from the radio halo. The pressure of the radio filaments listed in Table 5 are 3–5 times greater than the average thermal pressure of the ambient hot gas within the cooling core.

TABLE 5

RESULTS FROM ENERGY EQUIPARTITION ESTIMATES

Component	L_{6cm} (ergs s^{-1} Hz^{-1})	B_{min} (μG)	p_{min} (dyn cm^{-2})	t_{syn} (10^6 yr)	Size (kpc × kpc)
Core	1.6×10^{31}	200	2×10^{-9}	0.2	<0.3
Bipolar	1.6×10^{31}	20	5×10^{-11}	4	30 × 15
Halo	1.5×10^{31}	10	2×10^{-11}	9	75 × 45
Loop	8.7×10^{28}	30	9×10^{-11}	3	25 × 1.5
Filament	6.7×10^{28}	30	6×10^{-11}	4	20 × 2

In addition, the gas pressure of the optical emission-line region in the central part of UGC 9799 can be estimated. The electron density can be determined from observations of the relative intensities of two lines of the same ion emitted by different levels which have nearly the same excitation energy, such as [S II] lines at 6717 Å and 6731 Å (Heckman et al. 1989). Assuming $T_e = 10^4$ K and the S^+ zone is 50% ionized, the estimated pressure for the core ($r < 1$ kpc) is 1.7×10^{-9} dyn cm^{-2} (where r is a distance from the nucleus). The emission-line gas in the nucleus is almost two orders of magnitude greater than the minimum pressure of the extended radio plasma and the hot X-ray gas. It is not surprising that the pressure in the optical emission gas is higher since the radio and X-ray measurements are made at considerably larger distance from the nucleus. However, based on the observations of several cooling flow clusters, Heckman et al. (1989) found that the outer portions ($r > 2$ kpc) of the emission filaments tend to be in pressure equilibrium with the X-ray gas.

4. DISCUSSION

4.1. *Jets and Bipolar Flow*

Our new observations of 3C 317 confirm the lack of a well-defined jet morphology. The bipolar structure observed around the nucleus, however, suggests an outflow that may have been initially collimated to some degree. The lack of strong collimation could be due to a disruptive event in a jet flow on scales unresolved by the current observations. The cooling flow environment surrounding 3C 317 provides a possible mechanism for disrupting jets (e.g., Sumi, Norman, & Smarr 1988; Soker & Sarazin 1988).

Recently, Loken et al. (1993) numerically simulated a jet propagating in a cooling flow. They showed that jets with internal Mach numbers of 6–20 can be disrupted in a cooling flow. The key point of this disruption mechanism is the fast growing Kelvin-Helmholtz instability enhanced by the pressure and temperature gradients near the sonic point in the cooling flow (Loken et al. 1993; Zhao 1990) although the sonic point itself does not disrupt the collimation (Loken et al. 1993; Soker & Sarazin 1988).

If the cooling flow is transonic, the sonic radius may mark the region where the putative radio jets in 3C 317 become unstable. The estimated temperature in the cooling flow within the central 30 kpc of A2052 is approximately 1×10^7 K (Arnaud 1990). The mass accretion rate at this radius is approximately 20 $M_\odot$ yr^{-1}, assuming that the mass accretion rate decreases linearly with radius (Thomas, Fabian, & Nulsen 1987). An upper limit of the sonic radius can be estimated using the parameters derived from the X-ray data (Soker & Sarazin 1988):

$$r_s \leq 0.4 \text{ kpc} \left(\frac{\dot{M}_s}{1\ M_\odot\ \text{yr}^{-1}}\right)\left(\frac{T_s}{10^6\ \text{K}}\right)^{-2.6}, \qquad (1)$$

where $\dot{M}_s$ and T_s are the mass accretion rate and the temperature at the sonic radius. White & Sarazin (1987) showed that most of the cluster cooling flow models result in a small sonic radius $r_s < 1$ kpc. At subkiloparsec distance from the nucleus, the typical temperature decreases to a few times 10^6 K and the mass accretion rate is typically a few solar masses per year. Thus, the sonic point of A2052 is likely to be at a distance of <0.4 kpc from the core. This sonic point is consistent with the limits on the radio jet set by our current observations suggesting that the sonic disruption may be a plausible explanation to the absence of jets in a scale of ~ 1 kpc in 3C 317. However, it is worth noting that the sonic disruption mechanism is not a universal property of radio sources in central galaxies of cooling flow clusters (Soker & Sarazin 1988; Loken et al. 1993).

In addition, 3C 317 is a counterpart of 3C 84 in the center of the Perseus cluster which is believed to be associated with a cooling flow. 3C 84 is also characterized by an amorphous radio halo (Burns et al. 1992) and lack of well-collimated jets at kiloparsec scale (Pedlar et al. 1988). However, a disruptive parsec-scale jet has been observed with VLBI (e.g., Readhead et al. 1990). It will be important to observe the core of 3C 317 with the VLBA to determine if jets exist on a smaller scale.

4.2. *Radio Halo*

The inner bipolar structure in 3C 317 may be evidence that the remaining momentum in the disrupted outflow, which is probably subsonic, drives the radio plasma out from the nucleus along the initial collimated directions. The bipolar structure is, however, surrounded by a distinctive radio halo.

Further transport of relativistic electrons from the bipolar regions may be important in understanding the formation of the radio halo. There are two distinct transport mechanisms that we wish to consider: convection by the remaining momentum in the disrupted radio outflow or diffusion. The convection model (e.g., Learche & Schlikeiser 1981, 1982) predicts that, at frequencies below the break frequency, the spectral index is $\alpha = -0.5$. This value differs significantly from what has been observed at low frequencies ($\alpha = -0.8$). Thus, the transport of electrons in the halo by convections alone is probably not the principal process for 3C 317.

The diffusion process has been proposed as an important mechanism of transporting electrons in radio halo of galaxies as well as clusters (e.g., Jaffe 1977). The relativistic electrons wander along the magnetic field lines, scattering off Alfvén waves along the way. Because the field lines in clusters of galaxies are probably tangled (Hennessy, Owen, & Eilek 1989), the scattering of electrons is substantial. The relativistic electrons can propagate only after a density gradient is set up so they can diffuse down this density gradient. The stream of relativistic electrons will resonate with the Alfvén and hydromagnetic waves and transfer outward momentum to the waves, which slows down the propagation velocity and enhances the scattering. The mean free path is the characteristic length relevant to the diffusion process (e.g., Longair 1981). This mean free path is very short (~ 0.01 pc) in the radio halo. Thus, the relativistic electrons are strongly scattered in the cluster core region, and the propagation velocity of the particles through diffusion is approximately the Alfvén speed (Wentzel 1974) assuming that the ambient gas is fully ionized. For $B \sim 10\ \mu$G and $n_e \sim 0.01$ cm^{-3}, the inferred Alfvén speed is about 200 km s^{-1}.

There is evidence for spectral index breaks in all the extended source components as well as in the integrated flux densities of 3C 317. These spectral index breaks could be significant evidence for electron diffusion. If the electrons are injected continually from the nucleus, a steady state spectrum develops because outgoing high-energy electrons quickly lose their energy while the low-energy electrons travel farther out with proportionally less loss. Since the spectral break is evident even at distances of <15 kpc from the nucleus, electrons are losing substantial amounts of energy even in the bipolar component. Assuming that the spectrum above the break frequency, ν_B, steepens from the injected power law due to synchrotron losses, this break frequency is related to the electron age, t_s, and magnetic field, B, through the equation (e.g., Carilli et al. 1991)

$$t_s = 1.6 \times 10^3 \left(\frac{B}{1\ \mu\text{G}}\right)^{-3/2} \left(\frac{\nu_B}{1\ \text{GHz}}\right)^{-1/2} \text{Myr}\,. \qquad (2)$$

The typical age of the electrons is 70 Myr. The average diffusion velocity $\langle v_d \rangle$ is estimated by dividing the characteristic length that the electrons travel before losing their energy via synchrotron radiation, by the synchrotron lifetime, namely $\langle v_d \rangle \approx 15$ kpc/(7×10^7 yr) ≈ 200 km s^{-1}. This value agrees with what we estimated above for the Alfvén speed.

In addition, the magnitude of the spectral index break predicted by synchrotron aging is $\Delta\alpha \approx 0.5$ which is close to the observed value of 0.6 (e.g., Pacholzyk 1970).

Finally, the flat portion of the spectrum at $\nu < 0.5$ GHz is

-0.8, corresponding to an injection spectrum of $\gamma = 2.6$ ($\gamma = -2\alpha + 1$, assuming $N[E] \propto E^{-\gamma}$). This is a reasonable value according to shock acceleration theory (e.g., Bell 1978a, b; Blandford & Ostriker 1978) and is consistent with what is observed for the Galactic cosmic rays (e.g., Duric 1988).

Overall, the observed spectral characteristics and morphology of 3C 317 suggest that diffusion and synchrotron loss are the important physical processes in the radio halo.

4.3. *Origins of the Loop and Filaments*

Our new observations also show that the halo in 3C 317 is not featureless; rather, it is rich with filamentary structure. Similar filamentary structures have been observed in several other extragalactic radio sources such as Cyg A (Perley, Dreher, & Cowan 1984), 3C 310 (van Breugel & Fomalont 1984), M87 (Hines, Owen, & Eilek 1989), and Fornax A (Fomalont et al. 1989). Hines et al. (1989) have investigated synchrotron cooling, tearing instabilities, and hydrodynamic processes (turbulence and shocks) for creating these filamentary structures. As shown below, none of these processes seem well suited for the conditions in the halo of 3C 317.

In the case of synchrotron cooling instabilities, Hines et al. find that the resulting filaments will be dark, not bright as observed. This result is applicable to all radio sources, including 3C 317.

The tearing instability is the tendency for a plasma to break up into magnetic islands caused by the self-attraction of parallel currents in the resistive plasma. The addition of resistivity allows magnetic field lines to break and reconnect so that they are no longer frozen into the fluid as in ideal MHD where resistivity can be neglected. As the islands grow, the magnetic field lines are pulled in from above and below to weld together at the X-points and then tear apart to form the closed surfaces within the islands. In a non-zero resistivity plasma, filaments form and cause the magnetic field lines to bunch together. This instability may occur in cluster radio sources (Owen, Hardee, & Cornwell 1989). For the filaments in M87, Hines et al. find that the estimated instability time-scale is much longer than the synchrotron cooling time. In the absence of reacceleration, this instability leads to the production of dark filaments. Applying the tearing instability analysis to the loop and filaments in 3C 317, we find that the instability time scale ($t_{\rm tear} = 2.5 \times 10^{10}$ yr) is not only much longer than the synchrotron cooling time, but also of order the Hubble time. It seems that the process for breaking magnetic fields into filaments through the resistivity tearing instability is not effective to produce large-scale filaments in the radio halo of 3C 317.

Magnetic field reconnection through the resistive tearing process is too slow to produce discernible filaments in cluster radio sources. The effective speed of the reconnection process is $(v_{\rm A})/R_m$ (Parker 1979), where $v_{\rm A}$ is the Alfvén speed and $\sim R_m$ is the magnetic Reynolds number defined as the ratio of resistive diffusion time t_r to the Alfvén time $t_{\rm A}$. Alternatively, if the fluid is tenuous, the reconnection process proceeds more rapidly because the gas is compressed between the fields and less volume of fluid needs to be squeezed from between the fields (Petschek & Thorne 1967; Parker 1979). The merging speed of the fields could increase to order of $v_{\rm A}/\ln(R_m)$. The efficiency of the Alfvén merging rate is defined as $\epsilon = [\ln(R_m)]^{-1}$. Using η, a resistive diffusion coefficient, calculated by Hines et al., R_m is estimated as follows:

$$R_m \sim 9.4 \times 10^{12}\left(\frac{a}{\rm kpc}\right)\left(\frac{B}{10\ \mu{\rm G}}\right), \tag{3}$$

where a is the characteristic width of the filaments of loops. In the case of 3C 317, $a = 1$ kpc and $B = 10\ \mu$G, we estimate $\epsilon \sim 0.05$. Thus the time scale for this fast magnetic field reconnection is

$$t_{\rm rec} \approx \frac{a}{\epsilon v_a} \approx 9 \times 10^7\ {\rm yr}\left(\frac{\epsilon}{0.05}\right)^{-1}\left(\frac{a}{1\ {\rm kpc}}\right)\left(\frac{B}{10\ \mu{\rm G}}\right)^{-1}\left(\frac{n}{0.1\ {\rm cm}^{-3}}\right)^{1/2}. \tag{4}$$

This reconnection appears faster than the resistive tearing instability but is the same order as the lifetime of relativistic electrons due to synchrotron loss. The energy released by the reconnection of magnetic fields can reach 1×10^{43} ergs s^{-1} in the center of a cooling flow (Soker & Sarazin 1990), which may compensate for the energy loss by synchrotron radiation. The relativistic electrons generated by the reconnection can then interact with these fields and produce the filaments. This process may also produce filaments even when reconnection is unimportant for generating relativistic electrons. In this case, relativistic electrons generated by the first-order Fermi acceleration of diffusing relativistic electrons from the nucleus may interact with these fields. From the filaments in 3C 317, the coherence length needed would be of order 20 kpc. Roughly similar coherence lengths are inferred from Faraday rotation measurements of other radio sources at cluster centers (Hennessy et al. 1989). Filaments produced by coherent magnetic fields have been suggested for the radio arc in the Galactic center (Yusef-Zadeh, Morris, & Chance 1984). The coherence length of the magnetic field needed in the case of 3C 317 is, however, approximately 500 times larger.

Alternatively, filaments may be produced through Rayleigh-Taylor instabilities (Spitzer 1954) at the interface between the relativistic electron bubble and the cooling flow (Bohringer & Morfill 1988). If the active nucleus provides sufficient power to blow relativistic electron bubbles, the high-pressure gas (light) must be accelerating the ambient thermal gas (denser). The effect of gravity in the radio halo is negligible. The effective acceleraion due to the pressure gradient in the blowing bubbles can be estimated as

$$g \approx \frac{\nabla P}{\rho_{\rm amb}} \approx \frac{\bar{P}}{h\rho_{\rm amb}}, \tag{5}$$

where $\bar{P}$ is average pressure in the blowing bubbles and h is the height of the pressure gradient. $\rho_{\rm amb}$ is the mass density of the ambient gas. We adopt a value of 5×10^{-11} dyn cm^{-2}, an average pressure derived from the equipartition calculation (see § 3.6 and Table 5) for the relativistic electron bubble within a radius of 20 kpc from the nucleus, which is close to the thermal pressure derived from the X-ray data. For $\bar{P} = 5 \times 10^{-11}$ dyn cm^{-2}, $h = 20$ kpc, and $\rho_{\rm amb} = 1.5 \times 10^{-26}$ g cm^{-3}, the effective acceleration is $g \approx 5.4 \times 10^{-8}$ cm s^{-2} from equation (5). We estimate the growth time for the Rayleigh-Taylor instability as

$$t_{\rm RT} \approx 5.0 \times 10^5\ {\rm yr}\left(\frac{a_{\rm RT}}{\rm kpc}\right)^{1/2}\left(\frac{h}{\rm kpc}\right)^{1/2} \times \left(\frac{n_{\rm amb}}{10^{-2}\ {\rm cm}^{-3}}\right)^{1/2}\left(\frac{\bar{P}}{10^{-10}\ {\rm dyn\ cm}^{-2}}\right)^{-1/2}, \tag{6}$$

where $a_{\rm RT}$ is the typical width of RT filaments. For $h = 20$ kpc, $n_e = 0.01$ cm^{-3}, and $\bar{P} = 5 \times 10^{-11}$ dyn cm^{-2}, we find the

time scale $t_{RT} \sim 3 \times 10^6$ yr for $a_{RT} \sim 1$ kpc, a typical width of filaments. Since t_{RT} is less than the synchrotron cooling time, this analysis suggests that RT instabilities could be a possible process to form these radio filaments.

This Rayleigh-Taylor mechanism has been previously suggested for the production of optical emission line filaments in cooling flows (Bohringer & Morfill 1988). The extended optical emission line gas in 3C 317 is found to be cospatial with the radio halo (Baum et al. 1988), suggesting they may have a common origin. The fact that the extended optical emission filaments lie on the relatively dark regions of the radio emission (see Fig. 8) can be explained by using the Rayleigh-Taylor instability. This instability initially drives the hot intracluster medium to penetrate into the radio bubble while the bubble gas expands. The intracluster medium is further compressed by the high-pressure bubble gas to form high-density filaments. The high-density filaments cool more rapidly than ambient gas, and eventually, the high-density cooling gas collapses to discernible optical emission-line nebulae. If the magnetic fields are frozen in the gas, the collapse will enhance the magnetic fields in these clumps and the relativistic electrons will strongly scatter off significant Alfvén and hydromagnetic waves. Consequently, this causes rapid diffusion and synchrotron cooling of the relativistic electrons and prevents the radio gas from forming bright filaments in the region where the optical emission-line gas is located.

The high electron density of $n_e \approx 400$ cm^{-3} (Heckman et al. 1989) and short cooling and recombination time scales of $t_{rec} \sim 10^5 n_e^{-1}$ and $t_{cool} \sim 10^4 n_e^{-1}$ yr (Baum 1992) for the emission-line gas also suggest that the energy must be continually supplied to the filaments to maintain their temperature and ionization state (Baum 1992).

5. CONCLUSIONS

1. The radio halo of 3C 317 has been mapped in a great detail at wavelengths of 6, 20, and 90 cm using the VLA. A gradient in spectral indices at both 6/20 cm and 20/90 cm has been observed across the halo. The typical spectral index of the halo is -1.9 between the shorter wavelengths (6/20 cm), and the spectrum is significantly flattened at the longer wavelengths (20/90 cm) with a typical value of -1.5. The integrated spectrum of 3C 317 over a frequency range between 0.01 to 8 GHz shows a break around 0.5 GHz. A good fit to this spectrum has been obtained using two power laws with $\alpha = -1.4$ for $\nu > 0.5$ GHz and $\alpha = -0.8$ for $\nu < 0.5$ GHz. The amount of the spectral index change is $\Delta\alpha \sim 0.6$. The spectral characteristics and radio morphology suggest that diffusion, synchrotron losses and electron reacceleration are important in this radio halo.

2. In agreement with previous observations, the bipolar structure around the nucleus is observed but no jets have been detected with a resolution of 0".3. The bipolar structure suggests an outflow that may have been initially collimated to some degree. The lack of extended jets could be due to a disruptive event in a jet flow on scales unresolved by the VLA observations. It will be important to observe this nucleus using the VLBA in order to further investigate this possibility.

3. A wealth of filamentary structure has been revealed from our sensitive VLA observations. A radio emission loop (25 × 1.5 kpc) and large scale filaments (20 × 2 kpc), which connect to the bipolar structure, have been mapped with a resolution of 0".4 (0.4 kpc). The spectral indices ($\alpha \sim -1.5$) of these filamentary features appear less steep compared with the diffuse halo emission. The origins of these substructures have been discussed based on linear analysis of several instabilities. Either magnetic reconnection or Rayleigh-Taylor instability likely occurs in the radio halo to produce these filamentary structures.

In summary, the morphology and detailed structures seen in our new VLA maps of 3C 317 suggest a physical explanation that is substantially different from traditional models of collimated extragalactic radio sources (Begelman, Blandford, & Rees 1984). It is particularly intriguing to note the possible connection between the radio morphology and the cooling flow. As the possible prototype of a class of source associated with dominant galaxies in cooling cores, 3C 317 merits further theoretical modeling. Further high-resolution VLBA investigations may also help in understanding the energy transportation processes from the nucleus.

J.-H. Z. wishes to acknowledge the University of New Mexico for partial support during the course of this research. We thank T. M. Heckman for providing us with the optical emission-line data. We also thank C. Loken, C. Carilli, F. Owen, and J. Eilek for useful discussions. This work was supported in part from NSF grants AST-9012353 to J. O. B.

REFERENCES

Arnaud, K. A. 1990, private communication
Baars, J. W. M., Genzel, R., Pauliny-Toth, I. I. K., & Witzel, A. 1977, A&A, 61, 99
Baum, S. A. 1992, in Cluster & Superclusters of Galaxies, ed. A. C. Fabian (Dordrecht: Kluwer), 171
Baum, S. A., Heckman, T., Bridle, A., van Breugel, W., & Miley, G. 1988, ApJS, 68, 643
Begelman, M. C., Blandford, R. D., & Rees, M. J. 1984, Rev. Mod. Phys., 56, 255
Bell, A. R. 1978a, MNRAS, 182, 147
———. 1978b, MNRAS, 182, 443
Blandford, R. D., & Ostriker, J. P. 1978, ApJ, 221, L29
Bohringer, H., & Morfill, G. E. 1988, ApJ, 330, 609
Braude, S. Y., Megn, A. V., Sokolov, K. P., Tkachenko, A. P., & Sharykin, N. K. 1979, Ap&SS, 64, 73
Bridle, A. H., & Perley, A. P. 1984, ARA&A, 22, 319
Burns, J. O. 1990, AJ, 99, 14
Burns, J. O., Owen, F. N., & Rudnick, L. 1979, AJ, 84, 1683
Burns, J. O., Sulkanen, M. E., Gisler, G. R., & Perley, R. A. 1992, ApJ, 388, L49
Carilli, C. L., Perley, R. A., Dreher, J. W., & Leahy, J. P. 1991, ApJ, 383, 554
Clark, B. G. 1980, A&A, 89, 377
Cornwell, T. 1986, in Synthesis Imaging (NRAO Workshop 13), ed. R. A. Perley, F. R. Schwab, & A. H. Bridle (Green Bank: NRAO), 109
Duric, N. 1988, Space Sci. Rev., 48, 73
Edge, A. C., Stewart, G. C., & Fabian, A. C. 1992, MNRAS, 258, 177
Fabian, A. C., Nulsen, P. E., & Canizares, C. R. 1991, Astron. Astrophys. Rev., 2, 191
Faranoff, B. L., & Riley, J. M. 1974, MNRAS, 167, 31P
Fomalont, E. B., Ebneter, K. A., van Breugel, W. J. M., & Ekers, R. D. 1989, ApJ, 346, L17
Gubanov, A. G. 1985, AZh, 62, 1
Heckman, T., Baum, S., van Breugel, W., & McCarthy, P. 1989, ApJ, 338, 48
Hennessy, G., Owen, F. N., & Eilek, J. A. 1989, ApJ, 347, 144
Hines, D. C., Owen, F. N., & Eilek, J. A. 1989, ApJ, 347, 713
Jaffe, W. J. 1977, ApJ, 212, 1
Jones, C., & Forman, W. 1984, ApJ, 276, 38
Kellermann, K. I., Pauliny-Toth, I. I. K., & Williams, P. J. S. 1969, ApJ, 157, 1
Lerche, I., & Schlickeiser, R. 1981, Astrophys. Lett., 22, L31
———. 1982, A&A, 107, 148
Loken, C., Burns, J. O., Norman, M. L., & Clarke, D. A. 1993, ApJ, in press
Longair, M. S. 1981, High Energy Astrophysics (Cambridge: Cambridge Univ. Press)

Mills, B. Y., Slee, O. B., & Hill, E. R. 1958, Australian J. Phys., 11, 360
Owen, F. N., Hardee, P. E., & Cornwell, T. J. 1989, ApJ, 340, 698
Pacholczyk, A. G. 1970, Radio Astrophysics (San Francisco: Freeman)
Parker, E. N. 1979, Cosmical Magnetic Fields (Oxford: Clarendon Press)
Pedlar, A., Ghataure, H., Davies, R. D., Harrison, B., Perley, R., & Crane, P. C. 1988, in Cooling Flows in Clusters and Galaxies, ed. A. C. Fabian (Dorcrecht: Kluwer), 149
Perley, R. A., Dreher, J. W., & Cowan, J. J. 1984, ApJ, 285, L35
Petscheck, J. E., & Thorne, R. M. 1967, ApJ, 147, 1157
Readhead, A. C. S., Venturi, T., Marr, J. M., & Backer, D. C. 1990, in Parsec-Scale Radio Jets, ed. J. A. Zensus & T. J. Pearson (Cambridge: Cambridge Univ. Press), 71
Roland, J., Hanisch, R. J., Véron, P., & Fomalont, E. 1985, A&A, 148, 323
Sarazin, C. L. 1986, Rev. Mod. Phys., 58, 1
Sarazin, C. L., O'Connell, R. W., & McNamara, B. R. 1992, ApJ, 389, L59
Soker, N., & Sarazin, C. L. 1988, ApJ, 327, 66
———. 1990, ApJ, 348, 73
Spitzer, L. 1954, ApJ, 120, 1
Stewart, G. C., Canizares, C. R., Fabian, A. C., & Nulsen, P. E. J. 1984, ApJ, 278, 536
Stull, M. A. 1971, AJ, 76, 1
Sumi, D. M., Norman, M. L., & Smarr, L. L. 1988, in Cooling Flows in Clusters and Galaxies, ed. A. C. Fabian (Dordrecht: Kluwer), 257
Thomas, P. A., Fabian, A. C., & Nulsen, P. E. J. 1987, MNRAS, 228, 973
van Breugel, W., & Fomalont, E. B. 1984, ApJ, 282, L55
Viner, M. R., & Erickson, W. C. 1975, AJ, 80, 931
Wentzel, D. G. 1974, ARA&A, 12, 71
White, R. E., III, & Sarazin, C. L. 1987, ApJ, 318, 629
Williams, P. F. S., Collins, R. A., Caswell, F. L., & Holden, D. F. 1968, MNRAS, 139, 289
Wills, B. J. 1975, Australian J. Phys., Astrophys. Suppl., 38, 1
Yusef-Zadeh, F., Morris, M., & Chance, D. 1984, Nature, 310, 557
Zhao, J.-H. 1990, Ph.D. thesis, Univ. of New Mexico
Zhao, J.-H., Burns, J. O., & Owen, F. N. 1989, AJ, 98, 64

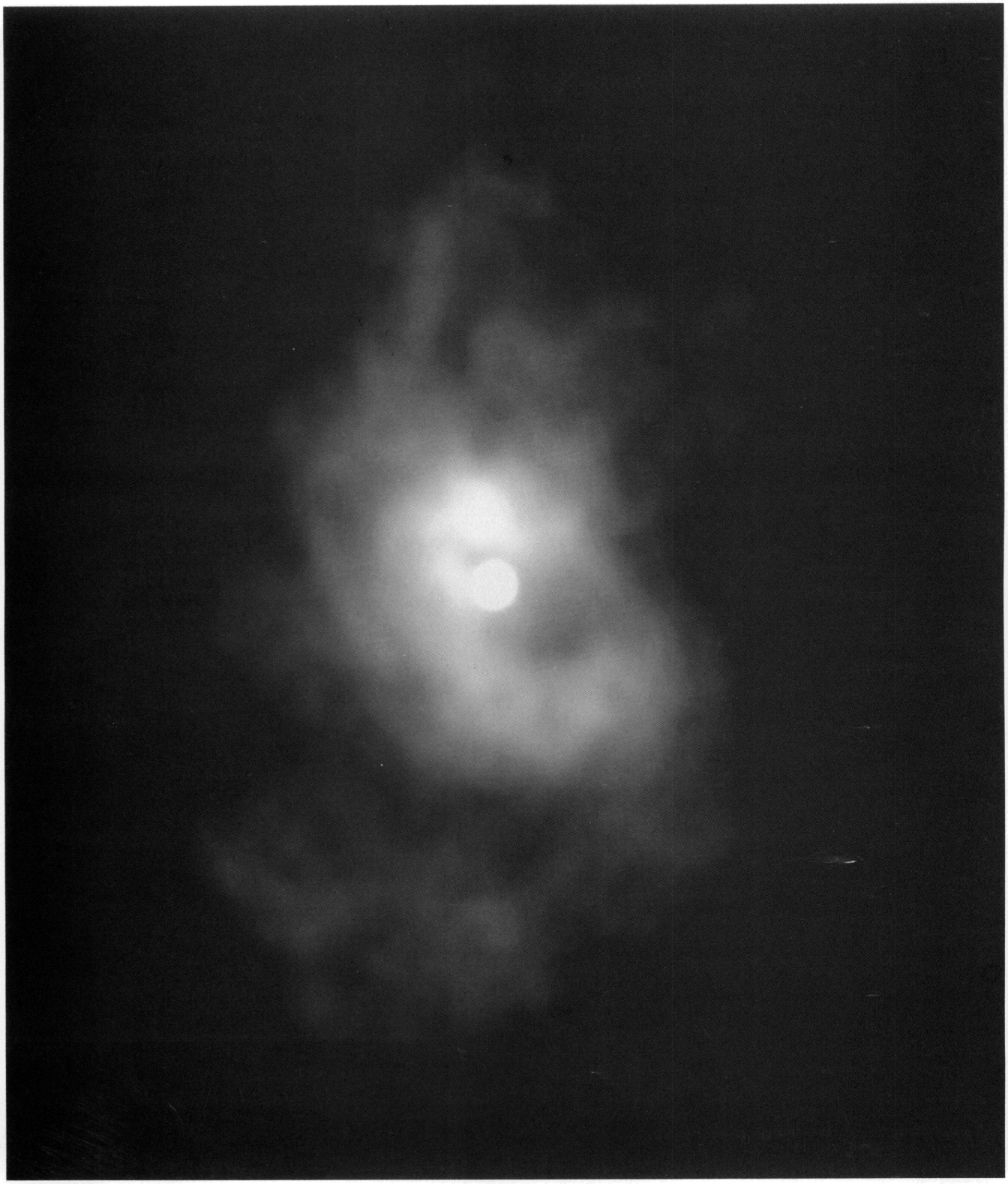

FIG. 2.—Gray-scale image of 3C 317 at 20 cm, showing a compact source at the center and the curved bipolar component surrounded by a diffuse halo. The filaments and loop seen in this image are also shown in 6 cm image (see Fig. 4). The image were convolved to 1″.4. A contour map of this image is shown in Fig. 3*b*.

ZHAO et al. (see 416, 52)